Journal of Hydrology 614 (2022) 128589

Contents lists available at ScienceDirect

Journal of Hydrology

journal homepage: www.elsevier.com/locate/jhydrol

Research papers

Analytical solutions for seawater intrusion and the maximum pumping rate of a well in unconfined coastal aquifers bounded by L-shaped coastlines

Jia Zhang [a,b], Chunhui Lu [a,b,*], Huiqiang Wu [a,b], Ling Li [c]

[a] State Key Laboratory of Hydrology-Water Resources and Hydraulic Engineering, Hohai University, Nanjing, China
[b] Yangtze Institute for Conservation and Development, Hohai University, Nanjing, China
[c] College of Engineering, Westlake University, Hangzhou, China

ARTICLE INFO

Keywords:
Well pumping
Analytical solution
L-shaped coastal boundary
Maximum pumping rate

ABSTRACT

Determining the maximum pumping rate (i.e., the maximum allowable pumping rate that does not cause seawater intrusion into the well under the steady-state condition) of a well is the key for sustainable management of coastal aquifers, as overexploitation of coastal aquifers could lead to the widespread occurrence of aquifer salinization (i.e., seawater intrusion). In this study, we develop steady-state analytical solutions to describe seawater intrusion and the maximum pumping rate of a well located in unconfined coastal aquifers bounded by L-shaped coastlines. Rectangular coastal aquifers bounded by two orthogonal constant-head boundaries (i.e., two coastlines) and two orthogonal no-flow inland boundaries are assumed in conceptual models, where replenishment of aquifers is via surface recharge. Analytical solutions are derived by the potential theory and the conformal mapping method, and validated by variable-density flow numerical simulations. It is found that analytical solutions based on the sharp-interface approximation overestimate seawater intrusion and underestimate the maximum pumping rate. An acceptable, conservative maximum pumping rate is obtained by using the correction factor proposed by Lu and Werner (2013). Moreover, the sensitivity of the well location on the maximum pumping rate is investigated, showing that an optimal well location exists. Analytical solutions developed in the current study provide a convenient tool for assessing pumping effects in coastal aquifers bounded by L-shaped coastlines, servicing to various management objectives.

1. Introduction

The impact of groundwater pumping on seawater intrusion in coastal areas has received increasing attention in recent decades, as overexploitation of coastal aquifers could lead to the widespread occurrence of aquifer salinization (i.e., seawater intrusion). Various management strategies, such as the injection-extraction well system, optimization of well placement and pumping rates, and subsurface barriers, have been proposed to enhance groundwater pumping under the threats of seawater intrusion (Park et al., 2009; Cheng et al., 2000; Lu et al., 2013; Shi et al., 2020; Wu et al., 2020).

Determination of the freshwater-seawater interface position requires that the flows in freshwater and interface zones are solved simultaneously to satisfy the continuity of pressure and flux. Though variable-density flow numerical simulations are capable for exploring various complex scenarios, the analytical method based on the sharp-interface approximation has been widely employed to explore how groundwater pumping affect seawater intrusion for simplified coastal settings (Cheng et al., 2000; Koussis et al., 2012). Analytical solutions for seawater intrusion based on the density-dependent system are only available for some simplified cases without pumping (Dentz et al., 2006; Bolster et al., 2007). The benefit of the analytical method lies in the simplicity and speediness, and hence it can serve as the first-order assessment tool. In addition, the analytical method is a useful tool for theoretical studies, as it can more easily reveal the underlying relationship between various variables.

The potential theory proposed by Strack (1976) gives a simple analytical tool to calculate the maximum safe pumping rate (i.e., the maximum allowable pumping rate that does not cause seawater intrusion into the well under the steady-state condition) of a single well in a semi-infinite homogeneous coastal aquifer. Later on, the analytical approach of Strack (1976) has been extended to explore multiple well scenarios. Park et al. (2009) derived the approximate maximum pumping rates or minimum injection rates to limit seawater intrusion to

* Corresponding author at: State Key Laboratory of Hydrology-Water Resources and Hydraulic Engineering, Hohai University, Nanjing, China.
E-mail address: clu@hhu.edu.cn (C. Lu).

https://doi.org/10.1016/j.jhydrol.2022.128589
Received 23 June 2022; Received in revised form 31 August 2022; Accepted 30 September 2022
Available online 29 October 2022

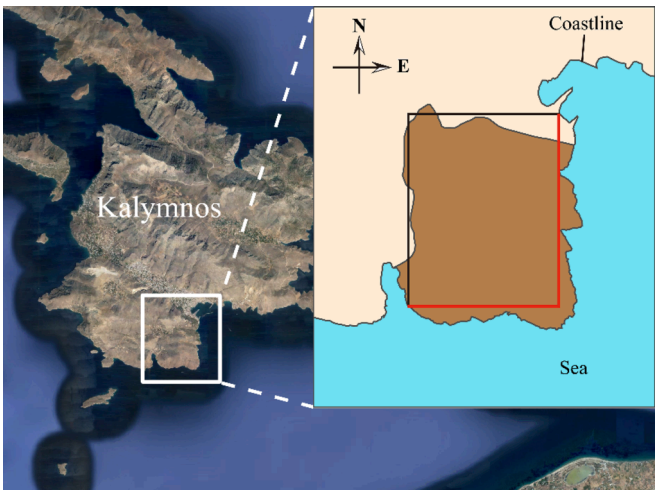

Fig. 1. Approximation of Kalymnos Island as an L-shaped coastline aquifer. The constant-head boundary and no-flow boundary are represented in red and black lines, respectively.

a prespecified distance from the coastline. Lu et al. (2013) developed an analytical solution of the maximum net groundwater extraction rate for their proposed injection-extraction well pair system in coastal aquifers. Recently, Shi et al. (2020) explored analytically the performance of multiple-well hydraulic barriers on enhancing groundwater extraction in a coastal aquifer, where one extraction well and two or three injection wells are considered.

In addition to multiple-well scenarios, the analytical method has been employed to investigate the effect of boundary conditions on coastal groundwater pumping. Mantoglou (2003) developed analytical models of seawater intrusion in coastal aquifers of finite size, which are then used to determine the maximum pumping rates by means of an optimization methodology. Lu et al. (2012) derived an analytical solution for evaluating maximum pumping rates in a domain with a constant-head inland boundary condition, where two lateral boundaries are considered at an infinite distance. Lu and Luo (2014) extended the study of Lu et al. (2012) by assessing additionally the role of lateral boundaries. Using the Schwartz-Christoffel conformal mapping method together with complex variable techniques, Lu et al. (2015) derived steady-state analytical solutions for pumping in a rectangular aquifer with four different combinations of impermeable and constant-head boundaries, and the usefulness of their developed analytical solutions was demonstrated by an application to well pumping in a finite coastal aquifer.

Despite these analytical studies mentioned above, they exclusively consider a straight coastline. In reality, however, a large number of bays, promontories and estuaries constitute a colorful shape of coastline. Fig. 1 shows the Greek island of Kalymnos, which can be approximated as an L-shape coastline aquifer. Actually, L-shaped coastline aquifers have been studied analytically to explore groundwater fluctuations under the tidal effects (e.g., Li et al., 2000; Li and Jiao, 2002; Li et al., 2002). Nevertheless, the analytical study on how groundwater pumping affects seawater intrusion in coastal aquifers bounded by L-shaped coastlines is currently unavailable. It is expected that this type of the coastal boundary would give rise to a significant effect on groundwater pumping.

In this study, we aim to derive the steady-state analytical solutions for the maximum pumping rate of a pumping well located in unconfined coastal aquifers bounded by L-shaped coastlines. Analytical solutions are developed based on the potential theory together with our previous analytical solutions derived for pumping in a rectangular aquifer (Lu et al., 2015). Variable-density flow numerical simulations are employed to validate the accuracy of developed analytical solutions.

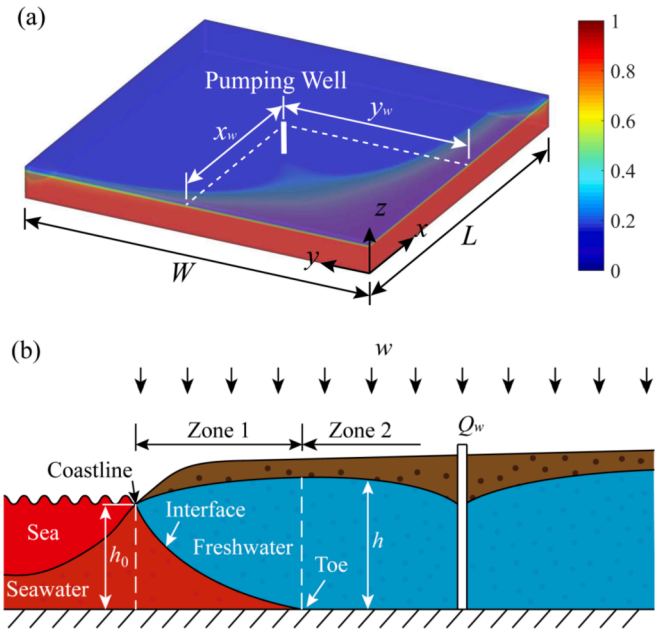

Fig. 2. Schematic description of the conceptual model: (a) model domain, and (b) section from the coastline to the pumping well. The color bar shows the normalized salinity distribution.

2. Conceptual model

We consider an isotropic, homogeneous, rectangular unconfined coastal aquifer with the hydraulic conductivity, K [L/T]. The seaward boundaries (constant-head) are two coastlines perpendicular to each other and the inland boundaries are two no-flow boundaries (e.g., groundwater divide, bedrock, or upthrown fault block of relatively impervious rock), as shown in Fig. 2a. The x-y axes have an origin at the horizontal impermeable basement of the aquifer where two coastlines meet, with positive x and y along both coastlines. The z axis is pointing upwards and the sea level is h_0 [L] above the aquifer basement. A constant pumping rate, Q_w [L^3/T], from a fully penetrating well occurs at distances x_w [L] and y_w [L] from the two coastlines, while spatially and temporally uniform recharge w [L/T] occurs over the whole domain with length, L [L], and width, W [L]. The densities of seawater and freshwater are ρ_s [ML^{-3}], and ρ_f [ML^{-3}], respectively.

To identify the region taking the density effect from the sea, the section from the coastline to the pumping well is divided into Zone 1 and Zone 2 as shown in Fig. 2b. Freshwater flows to the sea above the seawater wedge in Zone 1 (also called "interface flow"), while only freshwater can be found in Zone 2 (i.e., "freshwater flow").

3. Derivation of analytical solution

3.1. Potential theory for L-shaped coastline aquifers

The analytical solution for the water head in an L-shaped coastline aquifer with pumping and uniform recharge can be solved by the superposition principle combining with the potential theory proposed by Strack (1976). To apply the potential theory, the following assumptions should be made: (1) the mixing between seawater and freshwater is neglected, leading to the sharp interface to separate both fluids in Zone 1 (see Fig. 2b), (2) the toe location (where the seawater-freshwater interface intersects the impermeable boundary) is given by employing Ghyben-Herzberg relation (Badon Ghyben and Drabbe, 1888; Herzberg, 1901), and (3) the freshwater flow is essentially horizontal and the vertical flow is negligible according to Dupuit-Forchheimer assumption (Dupuit, 1863; Forchheimer, 1886).

Employing the potential theory of unconfined aquifer, the relation between the groundwater head, h, and the potential, Φ [L^3/T], in this unconfined coastal aquifer can be expressed as (Equations (29) and (30) in Strack (1976)):

$$\Phi_1 = \frac{1}{2}K(1+\alpha)(h-h_0)^2 \tag{1}$$

$$\Phi_2 = \frac{1}{2}Kh^2 - \frac{1}{2}K\left(1+\frac{1}{\alpha}\right)h_0^2 \tag{2}$$

where Φ_1 is the potential in Zone 1, and Φ_2 in Zone 2. α [-] is the ratio of the freshwater density to the density difference between seawater and freshwater (normally, a value of 40 is taken). h and h_0 are the piezometric head at (x, y) and at the coastal boundary, respectively. Therefore, the groundwater head at the seawater wedge toe is given as $(1+1/\alpha)h_0$ obtained from the Ghyben-Herzberg relation.

According to the superposition principle, the potential Φ is related to the head boundary, well pumping, and constant recharge (Koussis et al., 2012; Strack and Ausk, 2015), written as $\Phi = \Phi_h + \Phi_q + \Phi_r$, where Φ_h [L^3/T], Φ_q [L^3/T], and Φ_r [L^3/T] are the potentials corresponding to the three parts as mentioned. Obviously, the constant-head boundary in this conceptual model leads to $\Phi_h = 0$.

The potential caused by recharge in such an L-shaped coastline aquifer obeys the following governing equation:

$$\nabla^2\Phi_r = -w,\ 0<x<L,\ 0<y<W \tag{3}$$

where ∇^2 is the Laplace operator. This governing equation is a nonhomogeneous linear equation. The corresponding boundary conditions are given by:

$$\Phi_r(0,\ y) = \Phi_r(x,\ 0) = 0 \tag{4}$$

$$\left.\frac{\partial\Phi_r}{\partial x}\right|_{x=L} = \left.\frac{\partial\Phi_r}{\partial y}\right|_{y=W} = 0 \tag{5}$$

Equations (4) and (5) indicate that they are linear boundary conditions. The application of the double finite Fourier sine transform is considered based on the governing equation and boundary conditions, leading to the following expression for the solution:

$$\Phi_r = \sum_{m,n=0}^{\infty} A_{mn}\sin\frac{(\pi+2m\pi)x}{2L}\sin\frac{(\pi+2n\pi)y}{2W} \tag{6}$$

Substituting Equation (6) into (3) produces:

$$\sum_{m,n=0}^{\infty} A_{mn}\lambda_{mn}^2\sin\frac{(\pi+2m\pi)x}{2L}\sin\frac{(\pi+2n\pi)y}{2W} = w \tag{7}$$

where $\lambda_{mn}^2 = \left(\frac{\pi+2m\pi}{2L}\right)^2 + \left(\frac{\pi+2n\pi}{2W}\right)^2$. Using the orthogonality of $\left\{\sin\frac{(\pi+2m\pi)x}{2L}\sin\frac{(\pi+2n\pi)y}{2W}\right\}$ in $[0, L] \times [0, W]$ leads to:

$$\begin{aligned} A_{mn} &= \frac{4}{LW\lambda_{mn}^2}\int_0^L\int_0^W w\sin\frac{(\pi+2m\pi)x}{2L}\sin\frac{(\pi+2n\pi)y}{2W}dxdy \\ &= \frac{16w}{(\pi+2m\pi)(\pi+2n\pi)\lambda_{mn}^2} \end{aligned} \tag{8}$$

Substituting Equation (8) into (6) derives the function of Φ_r.

Lu et al. (2015) has developed steady-state analytical solutions for the discharge potential, where a pumping well located in a fully bounded rectangular confined aquifer with no recharge, using the Schwartz-Christoffel conformal mapping method. According to this method, the discharge potential Φ_q at (x, y) in z-plane for an L-shaped coastline aquifer equals to the discharge potential Ω [L^3/T] at (u, v) in conformal mapping w-plane, expressed as:

$$\Omega = \frac{Q_w}{4\pi}\ln\left\{\frac{\left[(u-u_w)^2+(v-v_w)^2\right]\left[(u-u_w)^2+(v+v_w)^2\right]}{\left[(u+u_w)^2+(v-v_w)^2\right]\left[(u+u_w)^2+(v+v_w)^2\right]}\right\} \tag{9}$$

where u_w and v_w are the coordinates of the well location in w-plane, corresponding to the well location x_w and y_w in z-plane. The relation between point (u, v) in w-plane and (x, y) in z-plane can be given by:

$$M = \frac{sn(x/C;\ \sqrt{m})dn(y/C;\ \sqrt{1-m})}{cn^2(y/C;\ \sqrt{1-m}) + msn^2(x/C;\ \sqrt{m})sn^2(y/C;\ \sqrt{1-m})} \tag{10}$$

$$N = \frac{cn(x/C;\ \sqrt{m})dn(x/C;\ \sqrt{m})sn(y/C;\ \sqrt{1-m})cn(y/C;\ \sqrt{1-m})}{cn^2(y/C;\ \sqrt{1-m}) + msn^2(x/C;\ \sqrt{m})sn^2(y/C;\ \sqrt{1-m})} \tag{11}$$

$$u = \sqrt{\frac{\sqrt{\left(M^2-N^2-1\right)^2+(2MN)^2}+\left(M^2-N^2-1\right)}{2}} \tag{12}$$

$$v = \sqrt{\frac{\sqrt{\left(M^2-N^2-1\right)^2+(2MN)^2}-\left(M^2-N^2-1\right)}{2}} \tag{13}$$

where *sn*, *cn*, and *dn* are the three kinds of Jacobi elliptic functions, representing *sine*, *cosine*, and *delta* amplitude elliptic functions, and they can be evaluated by the built-in functions of *Matlab*®. m and C depend on the ratio of L to W. It should be noted that the limitation of "crowding" problem needs L/W varying between 1/10.9 and 10.9/1 (Howell and Trefethen, 1990; Lu et al., 2015). The derivation for this mapping method is shown in Appendix A.

Therefore, substituting Equations (10), (11), (12), and (13) into (9), the potential Φ_q (equal to Ω) at (x, y) in z-plane can be given. The potential Φ for the L-shaped coastline aquifer is now obtained, since Φ_h, Φ_r and Φ_q have been developed. Substituting the value of Φ into Equations (1) and (2) produces the groundwater head distribution, h, in Zone 1 and Zone 2, respectively.

3.2. Maximum pumping rate

Since the stagnation point of the extraction well is the critical location to distinguish the capture zone (e.g., water in this zone will be extracted by the well), the maximum pumping rate occurs when the seawater wedge toe coincides with this point theoretically (Strack, 1976). An infinitesimal increase of pumping rate causes saltwater upconing.

To determine the maximum pumping rate, the coordinates of the stagnation point should be found first. For a given pumping rate Q_w, the partial differentials of the total potential Φ with respect to x and y equal to zero at the stagnation point. That is:

$$\left.\frac{\partial\Phi}{\partial x}\right|_{x=x_s} = 0 \tag{14}$$

$$\left.\frac{\partial\Phi}{\partial y}\right|_{y=y_s} = 0 \tag{15}$$

where x_s and y_s are the coordinates of the stagnation point. Note that multiple stagnation points may occur (depending on the well location and extraction rate) and when the well is close to the no-flow boundary, the stagnation point may occur at the no-flow boundary. The derivations of $\partial\Phi/\partial x$ and $\partial\Phi/\partial y$ are given in Appendix B. At the same time, the potential at the stagnation point $\Phi_s(x_s, y_s)$ is obtained by using the solution in Section 3.1. Substituting the head, $(1+1/\alpha)h_0$, at the seawater wedge toe into Equation (1), the potential at the toe location can be written as:

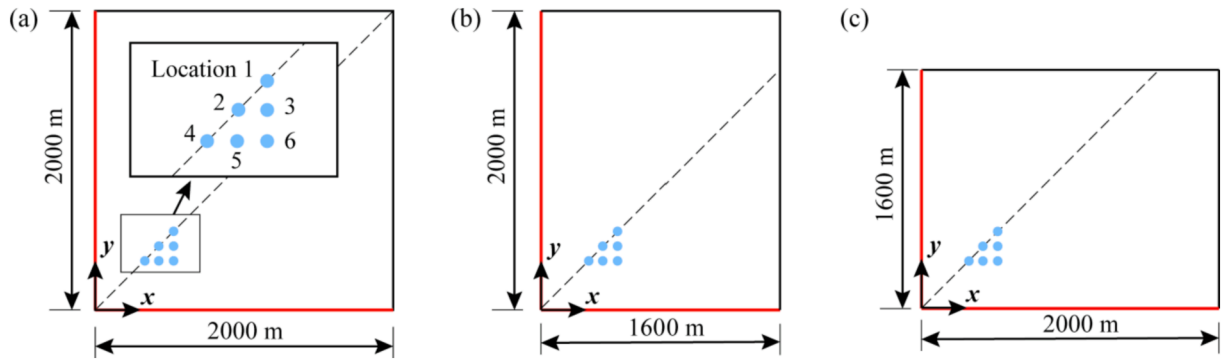

Fig. 3. Cases settings with three domain sizes for numerical validation: (a) Case S, $L = 2000$ m, $W = 2000$ m, (b) Case W, $L = 1600$ m, $W = 2000$ m, and (c) Case L, $L = 2000$ m, $W = 1600$ m. The coastline (constant-head boundary) is shown in red, while the two no-flow boundaries are represented in black. The dotted line shows the points where $x = y$. The well location coordinates: (Location 1: 604, 606), (Location 2: 500, 500), (Location 3: 604, 500), (Location 4: 404, 404), (Location 5: 500, 404), and (Location 6: 604, 404).

$$\Phi_{\text{Toe}} = \frac{(1+\alpha)K}{2\alpha^2} h_0^2 \tag{16}$$

Using an iterative procedure with an increasing value of Q_w, Φ_s gradually increases and finally the maximum pumping rate $Q_{\max}$ is determined when $\Phi_s = \Phi_{\text{Toe}}$.

3.3. Correction factor

In reality, a mixing zone develops between freshwater and seawater, which leads to the analytical non-dispersive solutions inconsistent with variable-density flow numerical simulation results. An empirical factor is proposed by Pool and Carrera (2011) to correct the density factor (α) and to overcome this issue. The corrected density factor (α^*) is given as:

$$\frac{1}{\alpha^*} = \frac{1}{\alpha}\left[1 - \left(\frac{\alpha_T}{B}\right)^c\right] \tag{17}$$

where α_T [L] is the transverse dispersivity and B [L] is the aquifer thickness. The empirical exponent c proposed by Pool and Carrera (2011) is 1/6, which is based on the pumping situation in flux-controlled confined aquifer systems, and the corrected analytical result matches the saline portion between 50 % and 75 % contour-lines. Lu and Werner (2013) found that c of 1/4 is better for locating 10 % seawater concentration in head-controlled coastal aquifers. For the comparison purpose, both values of correction factors are considered in our study.

4. Numerical validation

4.1. Description of Case setup

Fig. 3 shows three L-shaped coastline aquifers with different domain sizes, which are used to validate developed analytical solutions. Besides the square domain (i.e., Fig. 3a, $L \times W = 2000$ m $\times$ 2000 m, named Case S), larger width domain (i.e., Fig. 3b, $L \times W = 1600$ m $\times$ 2000 m, named Case W) and larger length domain (i.e., Fig. 3c, $L \times W = 2000$ m $\times$ 1600 m, named Case L) are also considered to ensure the generalization of a rectangular model domain. Each case has six pumping locations with coordinates of (Location 1: 604, 606), (Location 2: 500, 500), (Location 3: 604, 500), (Location 4: 404, 404), (Location 5: 500, 404), and (Location 6: 604, 404). Note that only one pumping well is considered at a time. Thus, there are six pumping situations for each model domain, resulting in that the total number of situations is eighteen. The sea level, h_0, in all cases is set to 30 m and the hydraulic conductivity, $K = 5$ m/d, is accepted. Seawater and freshwater densities, ρ_s and ρ_f, are 1025 kg/m^3, and 1000 kg/m^3, respectively. The recharge rate, w, is set as 0.0005 m/d, which is a common precipitation recharge in many coastal areas (e.g., Guo and Jiao, 2007; Werner et al., 2013).

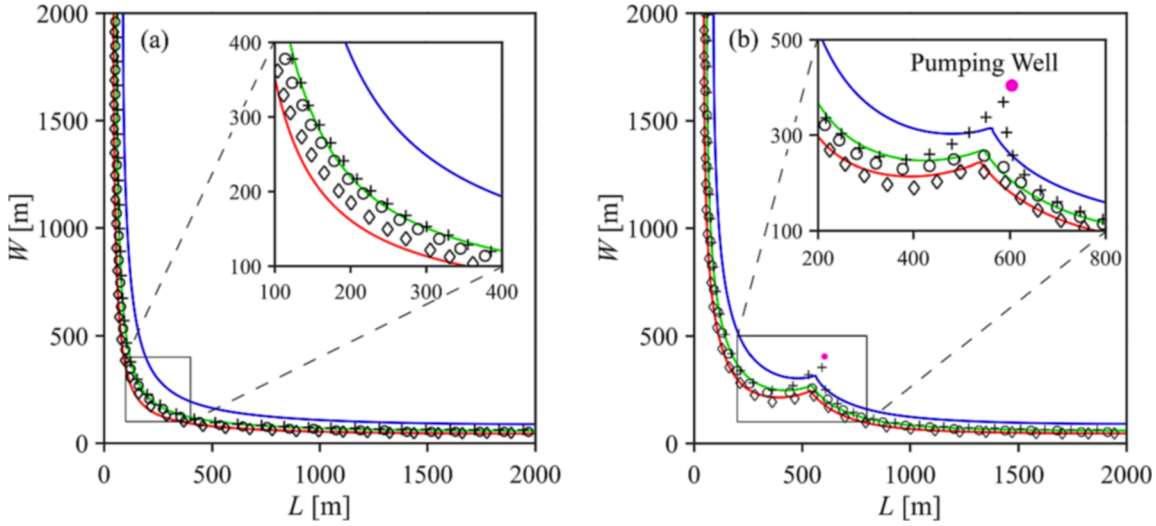

Fig. 4. Comparison of analytical and numerical results for the toe location in Case S: (a) steady state without pumping, and (b) with a maximum pumping rate at Location 6. The uncorrected analytical solution, and analytical solutions with a dispersion-corrected factor of 1/6 and 1/4 are represented by blue, red and green lines, respectively. The 10%, 50%, and 75% of seawater contour-lines obtained from the numerical results are marked by plus sign, circle, and diamond, respectively.

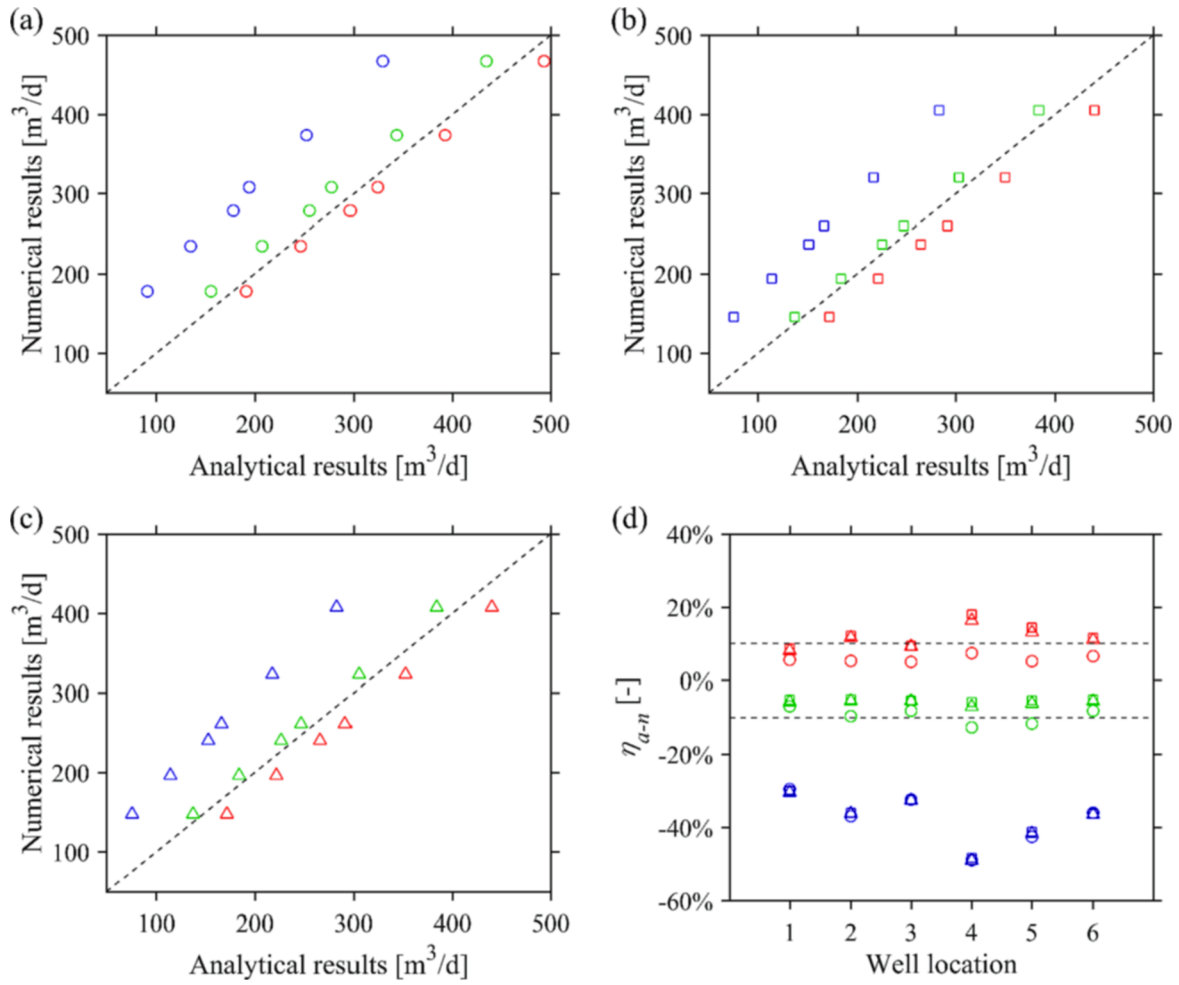

Fig. 5. The maximum pumping rates for: (a) Case S, (b) Case W, and (c) Case L, and (d) the relative maximum pumping rate between analytical and numerical results. The uncorrected analytical results, corrected analytical results with the factor of 1/6 and 1/4 are represented in blue, red and green, respectively. The black dotted lines in (d) are contours of $\eta_{a\text{-}n} = 10$ % and $\eta_{a\text{-}n} = -10$ %.

4.2. Numerical simulation setting

Analytical solutions developed are validated by numerical simulations using SEAWAT-2000 (Langevin and Guo, 2006). To ensure the accuracy in simulation, the grid Péclet criterion (Voss and Souza, 1987; Brovelli et al., 2007) should be satisfied, given as:

$$Pe = \frac{v\Delta L}{D_m + \alpha_L v} \approx \frac{\Delta L}{\alpha_L} \leqslant 4 \tag{18}$$

where D_m [L^2/T] is the molecular diffusion coefficient, ΔL [L] the grid spacing, and v [L/T] the magnitude of the local seepage velocity. The longitudinal and transverse dispersivity, α_L [L] and α_T [L], are set as 4 m, and 0.4 m, respectively. The grid size is 8 m long, 8 m width, and 3 m high, resulting in an acceptable Pe value of 2.92. Considering that the porosity does not affect the steady-state simulation (e.g., Robinson and Werner, 2017), it is set as 0.4, a typical value for unconfined aquifers in other numerical experiments (Lu et al., 2009; Bakhtyar et al., 2013). The simulation scenario is divided into two steps, including 100,000 days for the model running to a steady state without pumping, and then pumping 150,000 days to reach a new steady state. The salt concentration of seawater is constant and assigned as 35 kg/m^3 during the simulation. Head and salinity distributions are monitored to ensure that the steady state is achieved. To find the maximum pumping rate, various pumping rates are simulated until the steady average salinity in the extraction well is about 0.1 % (i.e., 35 mg/l, Pool and Carrera, 2011).

4.3. Comparison of analytical and numerical results

Case S is taken as an example to show the comparison between numerical concentration contour-lines and the analytical toe location, as shown in Fig. 4. Before pumping, the toe location calculated by the uncorrected analytical solution (i.e., the blue line) overestimates significantly the seawater extent obtained by the numerical simulation (see Fig. 4a), owing to the neglect of seawater energy loss resulting from the convection process between seawater and freshwater (Cooper, 1959; Dausman et al., 2010). As expected, the improved analytical toe location with a dispersion-corrected factor of 1/4 (Lu and Werner, 2013) and 1/6 (Pool and Carrera, 2011) are nearly match the 10 % and 75 % of seawater contour-lines, respectively.

After pumping, the corrected analytical solution with the correction factor of 1/6 approaches 50 % and 75 % contour-lines (see Fig. 4b). The analytical solution with the correction factor of 1/4 has a discernible difference in the toe location comparing with the 10 % seawater contour-line. Obviously, the 10 % contour-line of the numerical result is closer to the well than the analytical result using the correction factor of 1/4, particularly at locations near the pumping well. Moreover, we find that other simulation and analytical results for cases with different domain sizes and well locations have the similar tendency (not shown here).

The maximum pumping rates from analytical and numerical methods for eighteen scenarios are shown in Fig. 5a-5c. The relative difference of the maximum pumping rate between the analytical (Q_{ana})

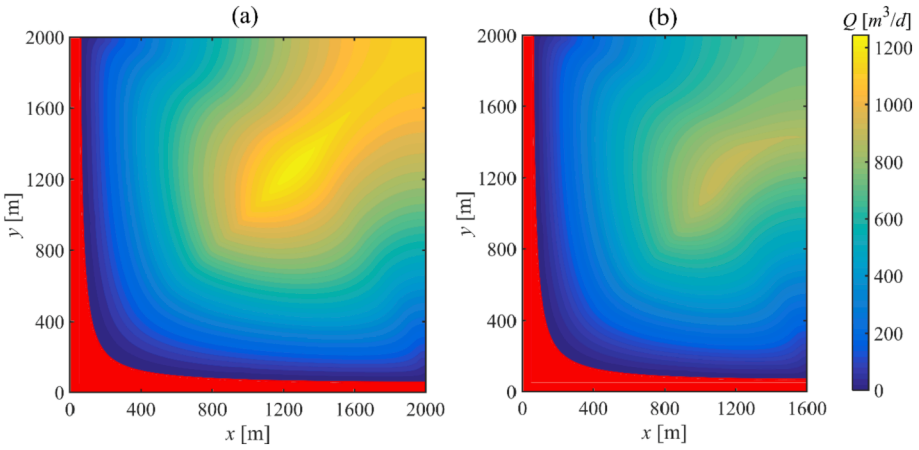

Fig. 6. The maximum pumping rates of an extraction well at different locations: (a) Case S, and (b) Case W. The red part indicates the seawater extent and no freshwater can be pumped by a well in this region.

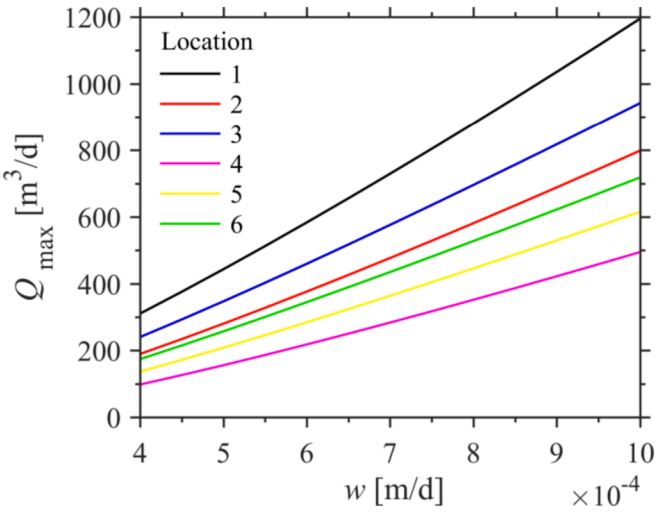

Fig. 7. The sensitivity of the maximum pumping rate to the recharge for wells in Case S.

and numerical (Q_{num}) results is calculated by $\eta_{a\text{-}n} = (Q_{ana} - Q_{num})/Q_{num}$, and shown in Fig. 5d. It is show that the corrected analytical solutions with either a factor of 1/4 or 1/6 improve the prediction accuracy, in comparison with the uncorrected analytical solution. For all cases, analytical solutions with the correction factor of 1/6 overestimate the maximum pumping rates. The overestimation of the maximum pumping rate using the correction factor of 1/6 has also been found by Kopsiaftis et al. (2019). By contrast, uncorrected analytical solutions and analytical solutions based on the correction factor of 1/4 underestimate the maximum pumping rates. From the angle of coastal groundwater management, a conservative value is often taken. In other words, the correction factor of 1/4 is more acceptable.

4.4. Sensitivity analysis

We choose the analytical solution with the correction factor of 1/4 to evaluate the maximum pumping rate of a well at different locations. Since Case W and Case L are symmetric with respect to $x = y$, the maximum pumping rates for the two cases are symmetric with respect to $x = y$. Therefore, we only show the results of Case S and Case W (see Fig. 6). The red part in Fig. 6 indicates the initial seawater extent, and thus no freshwater can be pumped at the location in this region. It is found that the largest values of the maximum pumping rates are 1243.6 m^3/d and 920.3 m^3/d for Case S and Case W, respectively, indicating the significance of the domain size impact. The larger domain size yields more abundant groundwater recharge, hence leading to higher exploitation potential.

The sensitivity of the maximum pumping rate to the recharge for wells in Case S is illustrated in Fig. 7. Similar increasing tendencies are found for Cases W and L (not shown here). As shown, the maximum pumping rate is smaller for the well closer to the coastline (decreasing from the symmetry axis to the coastline), if the distance between the well and one no-flow boundary is fixed (see Locations 1, 3 and 6 in the y-axis direction, and Locations 6, 5 and 4 in the x-axis direction). A larger recharge rate results in a larger maximum pumping rate, as expected.

5. Discussion

The analytical solution proposed by Strack (1976) provided a convenient approach for estimating the maximum pumping rate of a well in coastal aquifers with a straight coastline. This analytical solution has been extended to assess the maximum pumping rate in coastal aquifers with either multiple wells (injection and extraction wells) or complex boundary conditions (Lu et al., 2013; Lu and Luo, 2014; Lu et al., 2015; Shi et al., 2020). L-shaped coastlines are ubiquitous in real-world coastal aquifers, while the maximum pumping rate of a well in such aquifers is previously not available. The analytical solution presented in the current study provides a simple tool for quantifying seawater intrusion and the maximum pumping rate in coastal aquifers with L-shaped coastlines.

Due to the dispersion effect, there is a significant discrepancy between the uncorrected analytical solutions and numerical results. However, the empirical correction factor can greatly improve the accuracy of the analytical solution. The developed analytical solution can be extended to estimate the maximum pumping rate of a well in a multiple-well system by the superposition method, given that the pumping rates of other wells are known. For the optimization of the pumping rates of multiple wells, optimization methods such as genetic algorithm and artificial neural network are required (Cheng et al., 2000).

For a given coastal aquifer setting, the number and location of stagnation points caused by well pumping depend on the well location and the pumping rate. The stagnation point can occur within the aquifer domain or/and at the no-flow boundary. The critical stagnation point that first approaches the interface toe is either within the aquifer domain or at the no-flow boundary, leading to that the contour lines of the maximum pumping rate for a square aquifer domain are curvous (see Fig. 6a).

While the corrected analytical solutions well agree with the

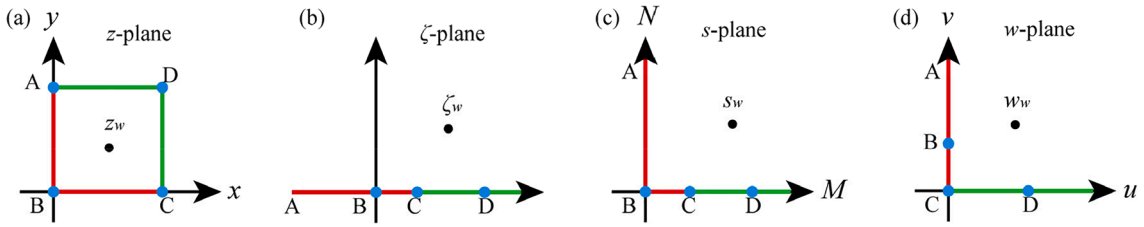

Fig. A1. The plane used for conformal mapping. The red and green lines indicate the constant head and no-flow boundary, respectively. The well is represented by the black circle.

numerical results, there are a number of limitations that surround the model assumption. First, the heterogeneity of the aquifer is neglected, while it exists in all real-world aquifer systems. Second, the aquifer is assumed to be recharged and extracted constantly and uniformly. In reality, however, the temporospatial patterns of recharge and pumping occur. Third, other transient factors, such as tides, waves, and evapotranspiration are not considered. Despite these limitations, the analytical solution developed offers a rapid assessment tool for first-pass estimation of pumping effects in coastal aquifers bounded by L-shaped coastlines.

6. Conclusions

Analytical solutions of the maximum pumping rate for a pumping well located in an L-shaped coastline aquifer have been derived in this study, relying on the potential theory and previous analytical solutions derived for pumping in a rectangular aquifer. Variable-density flow numerical simulations are carried out to validate the developed analytical solutions. The results indicate that analytical solutions based on a sharp-interface approximation generally overestimate seawater intrusion and underestimate the maximum pumping rate. A more acceptable and conservative maximum pumping rate is obtained by using a correction factor proposed by Lu and Werner (2013). Corrected analytical solutions provide a convenient tool for evaluating seawater intrusion and the maximum pumping rate in L-shaped coastline areas.

CRediT authorship contribution statement

Jia Zhang: Investigation, Methodology, Writing – original draft. **Chunhui Lu:** Conceptualization, Funding acquisition, Investigation, Resources, Supervision, Writing – review & editing. **Huiqiang Wu:** Investigation, Methodology. **Ling Li:** Investigation, Writing – review & editing.

Declaration of Competing Interest

The authors declare that they have no known competing financial interests or personal relationships that could have appeared to influence the work reported in this paper.

Data availability

No data was used for the research described in the article.

Acknowledgments

C. Lu acknowledges the financial support from the National Key Research and Development Project (2021YFC3200500), National Natural Science Foundation of China (51879088), Fundamental Research Funds for the Central Universities (B200204002), and Natural Science Foundation of Jiangsu Province (BK20190023).

Appendix A

Conformal mapping

Firstly, using Schwartz-Christoffel conformal mapping, the rectangular area in z-plane (Fig. A1a) is mapped to the upper half of ζ-plane (Fig. A1b) and the vertex A is signed as infinity on the real axis. The coordinates of the four vertices A, B, C, and D in the ζ-plane are: $\zeta_A = \infty$, $\zeta_B = 0$, $\zeta_C = 1$, and $\zeta_D = 1/m$ $(0 < m < 1)$. The transformation equation is given by:

$$z(\zeta) = C_1 \int \frac{1}{\sqrt{\zeta(\zeta-1)(\zeta-1/m)}} d\zeta + C_2 \tag{A1}$$

where C_1 relates to the size of the rectangle and C_2 equals to zero when the vertex B is set as the origin in both plane (i.e., $z_B = 0$, and $\zeta_B = 0$).

Secondly, the ζ-plane is transformed onto the s-plane (Fig. A1c) by letting $\zeta = s^2$. This transformation leads to the upper half of the ζ-plane mapped to the quarter of the s-plane. The coordinates of the vertices are $s_A \to \infty$, $s_B = 0$, $s_C = 1$, and $s_D = 1/m^{1/2}$. Thus, the transformation from z-plane to s-plane can be described as the following equation which is an incomplete elliptic integral of the first kind:

$$z(s) = C \int \frac{1}{\sqrt{(1-s^2)(1-ms^2)}} ds \tag{A2}$$

The distance between the vertices B ($z_B = 0$, $s_B = 0$) and C ($z_C = L$, $s_C = 1$) is written as:

$$L = z_C - z_B = C \int_0^1 \frac{1}{\sqrt{(1-s^2)(1-ms^2)}} ds \tag{A3}$$

Similarly, the distance between the vertices C ($z_C = L$, $s_C = 1$) and D ($z_D = L + iW$, $s_D = 1/m^{1/2}$) is produced:

$$iW = z_D - z_C = C \int_1^{1/\sqrt{m}} \frac{1}{\sqrt{(1-s^2)(1-ms^2)}} ds = iC \int_1^{1/\sqrt{m}} \frac{1}{\sqrt{(s^2-1)(1-ms^2)}} ds \tag{A4}$$

Assuming that $ms^2+(1-m)t^2=1$, which leads to $0 \le t \le 1$ when $1 \le s \le 1/m^{1/2}$, Equation (A4) can be modified as:

$$W = C\int_1^{1/\sqrt{m}} \frac{1}{\sqrt{(s^2-1)(1-ms^2)}}ds = C\int_0^1 \frac{1}{\sqrt{(1-t^2)[1-(1-m)t^2]}}dt \tag{A5}$$

Thus, parameters m and C subject to the following equations:

$$\frac{\int_0^1 \frac{1}{\sqrt{(1-s^2)(1-ms^2)}}ds}{\int_0^1 \frac{1}{\sqrt{(1-t^2)[1-(1-m)t^2]}}dt} = \frac{L}{W} \tag{A6}$$

$$C = \frac{L}{\int_0^1 \frac{1}{\sqrt{(1-s^2)(1-ms^2)}}ds} \tag{A7}$$

The relation between the s-plane and the z-plane follows the inverse function of Jacobi elliptic integrals. That is:

$$s = sn\left(\frac{z}{C}\right) \tag{A8}$$

where $s = M + iN$, and $z = x + iy$. sn is the *sine* amplitude elliptic function. Thus, the relation between (M, N) in s-plane and (x, y) in z-plane is obtained as:

$$M = \frac{sn(x/C;\ \sqrt{m})dn(y/C;\ \sqrt{1-m})}{cn^2(y/C;\ \sqrt{1-m}) + msn^2(x/C;\ \sqrt{m})sn^2(y/C;\ \sqrt{1-m})} \tag{A9}$$

$$N = \frac{cn(x/C;\ \sqrt{m})dn(x/C;\ \sqrt{m})sn(y/C;\ \sqrt{1-m})cn(y/C;\ \sqrt{1-m})}{cn^2(y/C;\ \sqrt{1-m}) + msn^2(x/C;\ \sqrt{m})sn^2(y/C;\ \sqrt{1-m})} \tag{A10}$$

in which *cn* and *dn* are the *cosine* and *delta* amplitude elliptic functions, respectively.

Finally, the s-plane is mapped onto the w-plane (Fig. A1d) to ensure the applicability of the superposition principle, through the transformation equation $w = (s^2-1)^{1/2}$. That is, the constant-head boundary and impermeable boundary are on the v axis and u axis of w-plane, respectively. The coordinates of the vertices are $w_A \to \infty$, $w_B = i$, $w_C = 0$, and $w_D = (1/m-1)^{1/2}$. The relation between (M, N) in s-plane and (u, v) in w-plane is:

$$u = \sqrt{\frac{\sqrt{(M^2-N^2-1)^2+(2MN)^2}+(M^2-N^2-1)}{2}} \tag{A11}$$

$$v = \sqrt{\frac{\sqrt{(M^2-N^2-1)^2+(2MN)^2}-(M^2-N^2-1)}{2}} \tag{A12}$$

Appendix B

Derivation of the partials of Φ with respect to x and y.

The potential Φ for L-shaped coastline aquifer considered is written as $\Phi = \Phi_r + \Phi_q + \Phi_h$ ($\Phi_h = 0$). Thus, the partial of Φ with respect to x is given as:

$$\frac{\partial\Phi}{\partial x} = \frac{\partial\Phi_r}{\partial x} + \frac{\partial\Phi_q}{\partial x} \tag{B1}$$

where $\partial\Phi_r/\partial x$ and $\partial\Phi_q/\partial x$ have the following expressions:

$$\frac{\partial\Phi_r}{\partial x} = \sum_{m,n=0}^{\infty} \frac{8w}{(\pi+2n\pi)L\lambda_{mn}^2}\cos\frac{(\pi+2m\pi)x}{2L}\sin\frac{(\pi+2n\pi)y}{2W} \tag{B2}$$

$$\begin{aligned}\frac{\partial\Phi_q}{\partial x} = {} & \frac{Q_w}{2}\left[\frac{\frac{\partial u}{\partial x}(u-u_w)+\frac{\partial v}{\partial x}(v-v_w)}{(u-u_w)^2+(v-v_w)^2} + \frac{\frac{\partial u}{\partial x}(u-u_w)+\frac{\partial v}{\partial x}(v+v_w)}{(u-u_w)^2+(v+v_w)^2}\right] \\ & -\frac{Q_w}{2}\left[\frac{\frac{\partial u}{\partial x}(u+u_w)+\frac{\partial v}{\partial x}(v-v_w)}{(u+u_w)^2+(v-v_w)^2} + \frac{\frac{\partial u}{\partial x}(u+u_w)+\frac{\partial v}{\partial x}(v+v_w)}{(u+u_w)^2+(v+v_w)^2}\right]\end{aligned} \tag{B3}$$

in which u and v are the function of M and N (i.e., Equations (A11) and (A12)). $\partial u/\partial x$ and $\partial v/\partial x$ are expressed as:

$$\frac{\partial u}{\partial x} = \frac{1}{4\sqrt{\gamma_1}}\left(\frac{1}{2\sqrt{\beta}}\frac{\partial\beta}{\partial x} + \frac{\partial\alpha}{\partial x}\right) \tag{B4}$$

$$\frac{\partial v}{\partial x}=\frac{1}{4\sqrt{\gamma_2}}\left(\frac{1}{2\sqrt{\beta}}\frac{\partial \beta}{\partial x}-\frac{\partial \alpha}{\partial x}\right) \tag{B5}$$

where $\alpha = M^2 - N^2 - 1$, $\beta = \alpha^2 + 4M^2N^2$, $\gamma_1 = (\alpha + \beta^{1/2})/2$, and $\gamma_2 = (-\alpha + \beta^{1/2})/2$. $\partial\alpha/\partial x$ and $\partial\beta/\partial x$ are obtained from following two equations:

$$\frac{\partial \alpha}{\partial x}=2M\frac{\partial M}{\partial x}-2N\frac{\partial N}{\partial x} \tag{B6}$$

$$\frac{\partial \beta}{\partial x}=2\alpha\frac{\partial \alpha}{\partial x}+8MN^2\frac{\partial M}{\partial x}+8M^2N\frac{\partial N}{\partial x} \tag{B7}$$

$\partial M/\partial x$ and $\partial N/\partial x$ are given by using Jacobi elliptic functions:

$$\begin{aligned}\frac{\partial M}{\partial x}=&\frac{cn(x/C,\sqrt{m})dn(x/C,\sqrt{m})dn\left(y/C,\sqrt{1-m}\right)}{C\left[cn^2\left(x/C,\sqrt{m}\right)+msn^2\left(x/C,\sqrt{m}\right)sn^2\left(y/C,\sqrt{1-m}\right)\right]}\\&-\frac{2msn^2\left(x/C,\sqrt{m}\right)cn\left(x/C,\sqrt{m}\right)dn\left(x/C,\sqrt{m}\right)sn^2\left(y/C,\sqrt{1-m}\right)dn\left(y/C,\sqrt{1-m}\right)}{C\left[cn^2\left(x/C,\sqrt{m}\right)+msn^2\left(x/C,\sqrt{m}\right)sn^2\left(y/C,\sqrt{1-m}\right)\right]^2}\end{aligned} \tag{B8}$$

$$\begin{aligned}\frac{\partial N}{\partial x}=&-\frac{sn(x/C,\sqrt{m})dn^2\left(x/C,\sqrt{m}\right)sn\left(y/C,\sqrt{1-m}\right)cn\left(y/C,\sqrt{1-m}\right)}{C\left[cn^2\left(x/C,\sqrt{m}\right)+msn^2\left(x/C,\sqrt{m}\right)sn^2\left(y/C,\sqrt{1-m}\right)\right]}\\&-\frac{msn(x/C,\sqrt{m})cn^2\left(x/C,\sqrt{m}\right)sn\left(y/C,\sqrt{1-m}\right)cn\left(y/C,\sqrt{1-m}\right)}{C\left[cn^2\left(x/C,\sqrt{m}\right)+msn^2\left(x/C,\sqrt{m}\right)sn^2\left(y/C,\sqrt{1-m}\right)\right]}\\&-\frac{2msn(x/C,\sqrt{m})cn^2\left(x/C,\sqrt{m}\right)dn^2\left(x/C,\sqrt{m}\right)sn^3\left(y/C,\sqrt{1-m}\right)cn\left(y/C,\sqrt{1-m}\right)}{C\left[cn^2\left(x/C,\sqrt{m}\right)+msn^2\left(x/C,\sqrt{m}\right)sn^2\left(y/C,\sqrt{1-m}\right)\right]^2}\end{aligned} \tag{B9}$$

The partial differential of Φ with respect to y is obtained using the symmetry of the coordinate (x, y) in z-plane and (X, Y) in Z-plane, which satisfies $X = y$ and $Y = x$. Thus, $\partial\Phi/\partial y$ equals to $\partial\Phi/\partial X$ and can be solved by Equations (B1) to (B9) (m and C require recalculation since the values of L and W are exchanged).

References

Badon Ghyben, W., Drabbe, J., 1888. Nota in verband met de voorgenomen putboring nabij Amsterdam (Note concerning the intended well drilling near Amsterdam). Tijdschr. van het K. Inst. van Ingenieurs 8–22.

Bakhtyar, R., Brovelli, A., Barry, D.A., Robinson, C., Li, L., 2013. Transport of variable-density solute plumes in beach aquifers in response to oceanic forcing. Adv. Water Resour. 53, 208–224. https://doi.org/10.1016/j.advwatres.2012.11.009.

Bolster, D.T., Tartakovsky, D.M., Dentz, M., 2007. Analytical models of contaminant transport in coastal aquifers. Adv. Water Resour. 30, 1962–1972. https://doi.org/10.1016/j.advwatres.2007.03.007.

Brovelli, A., Mao, X., Barry, D.A., 2007. Numerical modeling of tidal influence on density-dependent contaminant transport. Water Resour. Res. 43, W10426. https://doi.org/10.1029/2006WR005173.

Cheng, A.H.D., Halhal, D., Naji, A., Ouazar, D., 2000. Pumping optimization in saltwater-intruded coastal aquifers. Water Resour. Res. 36, 2155–2165. https://doi.org/10.1029/2000WR900149.

Cooper, H.H., 1959. A hypothesis concerning the dynamic balance of fresh water and salt water in a coastal aquifer. J. Geophys. Res. 64, 461–467. https://doi.org/10.1029/JZ064i004p00461.

Dausman, A.M., Langevin, C.D., Bakker, M., Schaars, F., 2010. A comparison between SWI and SEAWAT - The importance of dispersion, inversion and vertical anisotropy. 21st Salt Water Intrusion Meeting, Gov. of Azores, Azores.

Dentz, M., Tartakovsky, D.M., Abarca, E., Guadagnini, A., Sanchez-Vila, X., Carrera, J., 2006. Variable-density flow in porous media. J. Fluid Mech. 561, 209–235. https://doi.org/10.1017/S0022112006000668.

Dupuit, J., 1863. Études Théoriques et Pratiques sur le Mouvement des Eaux dans les Canaux Decouverts et à Travers les Terrains Perméables, 2ième ed. Dunod, Paris.

Forchheimer, P., 1886. Ueber die Ergiebigkeit von Brunnen-Anlagen und 718 Sickerschlitzen. Z. Architkt. Ing. Verlag 32, 539–563.

Guo, H., Jiao, J.J., 2007. Impact of coastal land reclamation on ground water level and the sea water interface. Ground Water 45, 362–367. https://doi.org/10.1111/j.1745-6584.2006.00290.x.

Herzberg, A., 1901. Die Wasserversorgung einer Nordseebaden [Water supply of a few hydrothermal spas in the North Sea]. J. Gasbeleucht Wasserversorg 44, 815–819.

Howell, L.H., Trefethen, L.N., 1990. A modified Schwarz-Christoeffel transformation for elongated regions. SIAM J. Sci. Stat. Comput. 11, 928–949. https://doi.org/10.1137/0911054.

Kopsiaftis, G., Christelis, V., Mantoglou, A., 2019. Comparison of sharp interface to variable density models in pumping optimisation of coastal aquifers. Water Resour. Manag. 33, 1397–1409. https://doi.org/10.1007/s11269-019-2194-7.

Koussis, A.D., Mazi, K., Destouni, G., 2012. Analytical single-potential, sharp-interface solutions for regional seawater intrusion in sloping unconfined coastal aquifers, with pumping and recharge. J. Hydrol. 416–417, 1–11. https://doi.org/10.1016/j.jhydrol.2011.11.012.

Langevin, C.D., Guo, W., 2006. MODFLOW/MT3DMS-based simulation of variable-density ground water flow and transport. Ground Water 44, 339–351. https://doi.org/10.1111/j.1745-6584.2005.00156.x.

Li, L., Barry, D.A., Cunningham, C., Stagnitti, F., Parlange, J.-Y., 2000. A two-dimensional analytical solution of groundwater response to tidal loading in an estuary and ocean. Adv. Water Resour. 23, 825–833. https://doi.org/10.1016/S0309-1708(00)00016-6.

Li, H., Jiao, J.J., Luk, M., Cheung, K., 2002. Tide-induced groundwater level fluctuation in coastal aquifers bounded by L-shaped coastlines. Water Resour. Res. 38, 6-1-6-8. 10.1029/2001WR000556.

Li, H., Jiao, J.J., 2002. Tidal groundwater level fluctuations in L-shaped leaky coastal aquifer system. J. Hydrol. 268, 234–243. https://doi.org/10.1016/S0022-1694(02)00177-4.

Lu, C., Kitanidis, P.K., Luo, J., 2009. Effects of kinetic mass transfer and transient flow conditions on widening mixing zones in coastal aquifers. Water Resour. Res. 45, W12402. https://doi.org/10.1029/2008WR007643.

Lu, C., Chen, Y., Luo, J., 2012. Boundary condition effects on maximum groundwater withdrawal in coastal aquifers. Ground Water 50, 386–393. https://doi.org/10.1111/j.1745-6584.2011.00880.x.

Lu, C., Luo, J., 2014. Groundwater pumping in head-controlled coastal systems: The role of lateral boundaries in quantifying the interface toe location and maximum pumping rate. J. Hydrol. 512, 147–156. https://doi.org/10.1016/j.jhydrol.2014.02.034.

Lu, C., Werner, A.D., 2013. Timescales of seawater intrusion and retreat. Adv. Water Resour. 59, 39–51. https://doi.org/10.1016/j.advwatres.2013.05.005.

Lu, C., Werner, A.D., Simmons, C.T., Robinson, N.I., Luo, J., 2013. Maximizing net extraction using an injection-extraction well pair in a coastal aquifer. Ground Water 51, 219–288. https://doi.org/10.1111/j.1745-6584.2012.00973.x.

Lu, C., Xin, P., Li, L., Luo, J., 2015. Steady state analytical solutions for pumping in a fully bounded rectangular aquifer. Water Resour. Res. 51, 8294–8302. https://doi.org/10.1002/2015WR017019.

Mantoglou, A., 2003. Pumping management of coastal aquifers using analytical models of saltwater intrusion. Water Resour. Res. 39, 1335. https://doi.org/10.1029/2002WR001891.

Park, N., Cui, L., Shi, L., 2009. Analytical design curves to maximize pumping or minimize injection or minimize injection in coastal aquifers. Ground Water 47, 797–805. https://doi.org/10.1111/j.1745-6584.2009.00589.x.

Pool, M., Carrera, J., 2011. A correction factor to account for mixing in Ghyben-Herzberg and critical pumping rate approximations of seawater intrusion in coastal aquifers. Water Resour. Res. 47, W05506. https://doi.org/10.1029/2010WR010256.

Robinson, N.I., Werner, A.D., 2017. On concentrated solute sources in faulted aquifers. Adv. Water Resour. 104, 255–270. https://doi.org/10.1016/j.advwatres.2017.04.008.

Shi, L., Lu, C., Ye, Y., Xie, Y., Wu, J., 2020. Evaluation of the performance of multiple-well hydraulic barriers on enhancing groundwater extraction in a coastal aquifer. Adv. Water Resour. 144, 103704 https://doi.org/10.1016/j.advwatres.2020.103704.

Strack, O.D.L., 1976. A single-potential solution for regional interface problems in coastal aquifers. Water Resour. Res. 12, 1165–1174. https://doi.org/10.1029/WR012i006p01165.

Strack, O.D.L., Ausk, B.K., 2015. A formulation for vertically integrated groundwater flow in a stratified coastal aquifer. Water Resour. Res. 51, 6756–6775. https://doi.org/10.1002/2015WR016887.

Voss, C.I., Souza, W.R., 1987. Variable density flow and solute transport simulation of regional aquifers containing a narrow freshwater-saltwater transition zone. Water Resour. Res. 23, 1851–1866. https://doi.org/10.1029/WR023i010p01851.

Werner, A.D., Zhang, Q., Xue, L., Smerdon, B.D., Li, X., Zhu, X., Yu, L., Li, L., 2013. An initial inventory and indexation of groundwater mega-depletion cases. Water Resour. Manag. 27, 507–533. https://doi.org/10.1007/s11269-012-0199-6.

Wu, H., Lu, C., Kong, J., Werner, A.D., 2020. Preventing seawater intrusion and enhancing safe extraction using finite-length, impermeable subsurface barriers: 3D analysis. Water Resour. Res. 56, e2020WR027792. 10.1029/2020WR027792.